

An Alternative Method to Optimize Mirrors Positions in Linear Fresnel Reflector

Elmaanaoui Youssef*, Saifaoui Dennoun

Laboratory of Renewable Energies and Systems Dynamics, faculty of sciences Ain Chock, Hassan II University of Casablanca,
Casablanca, Morocco.

*Corresponding author: elmaanaouiyoussef@gmail.com

Received: 23.03.2017 Accepted:02.05.2017

Abstract- Linear Fresnel Reflector (LFR) is regarded to as a promising Concentrated Solar Power technology (CSP). However, it suffers from low optical efficiency affected by optical losses such as blocking and shading. To overcome these problems, this study presents an alternative method to optimize mirrors positions in the LFR solar field in order to enhance its optical efficiency through the reduction of shading losses. This purpose is fulfilled by the calculation of the right spacing between adjacent mirrors to avoid mutual shading at a given Design Profile Angle (DPA). The comparison conducted between our method and a previously published one showed a good match between obtained results proving the validity of the work presented herein. After that, the impact of our alternative method on the optical behavior of the LFR, on the geometrical aspects of the solar field, and on energy production of the system is analyzed. Results showed that the whole process of developing new complex methods to optimize mirrors positions in the solar field is questionable. Instead, the authors think the use of simple equidistant spacing between adjacent mirrors is sufficient to reach satisfying results.

Keywords: Linear Fresnel Reflector; shading; blocking; design profile angle.

1. Introduction

Linear Fresnel Reflector (LFR) is a particular Concentrated Solar Power (CSP) technology that is expected to play an important role in the future [1]–[6]. An LFR system consists of several rows of flat or slightly bent reflecting mirrors installed near the ground. These mirrors track the sun on one axis to reflect sunrays on a receiver mounted few meters above the primary mirrors. This LFR simple structure gives it some interesting advantages over the other CSP technologies: it benefits from low wind drag effect [5], uses inexpensive mirrors that are easier to clean [7]–[13], uses fixed single receiver for the whole array [2], [7], [10], [12]. Due to all aforementioned advantages, LFR benefits from low capital and maintenance costs [4]–[6], [13]–[19].

Meanwhile, LFR captures less energy than the other CSP technologies making it less efficient [4], [11], [20], [21]. This

poor optical efficiency is due to shading, blocking, cosine effect, and end-loss [2], [22]–[26], [34]:

- Shading appears when a reflecting mirror find itself under the shadow of the neighboring one.
- Blocking appears when reflected sunrays of a mirror are intercepted by the adjacent one instead of being collected at the receiver.
- End-loss represents the part of the receiver that remains non-illuminated by the reflected sunrays.
- Cosine effect describes the amount of solar irradiance lost due to the reflecting mirrors not being perpendicular to the incidence sunlight.

During the past few years, LFR has been subject to numerous published papers that focus on the optimization of its optical and thermal performances. R. Abbas and J. M. Martínez-Val used curved mirrors with variable shift and width to study shading and blocking to improve the LFR efficiency without

increasing its cost [2]. They achieved a 1.2% increase in the power output using curved mirrors designed according to a sun reference. Abbas et al. compared in their work four different shapes of mirrors that have the same width and shift [8]. They concluded that the best shape to use is the cylindrical with specific design, even though parabolic shape had comparable results. J.D. Nixon and P.A. Davis presented a method to optimize LFR's optical efficiency through the avoidance of shading in the solar field. This was achieved using flat mirrors of the same width but with variable shift [6]. They reported an increase of 9% in the exergy averaged over the year with 122 additional hours of operation per year. Nixon et al. developed a novel LFR concept they called the Elevation LFR that reached an annual optical efficiency of 49% and an increase of 13-23% in exergy [27]. Moreover, it increased the operational hours by 9-24% and reduced land usage by 16-25%. Meanwhile, it is more complex and increased the capital cost. J. Chaves and M. Collares-Pereira also developed a novel LFR concept giving the solar field a wave-shape using variable size and shape of mirrors as well as multiple receivers [28]. They reported that concentrations as high as 85% of the theoretical maximum can be reached.

In this work, the authors chose to contribute to the undergoing efforts to optimize the LFR performances through the development of an alternative method to optimize mirrors positions in the solar field. The idea behind this method is to maximize the optical efficiency of the LFR by reducing shading losses in the solar field. This is achieved by finding the appropriate spacing between adjacent rows to avoid mutual shading between reflecting mirrors at a specific design profile angle. To prove the validity of the obtained results, a comparison is made with the method published by J.D. Nixon and P.A. Davis in [6].

A detailed discussion of the principles and the mathematical foundations of our alternative method is presented in the following section alongside with the methodology used to evaluate shading and blocking efficiencies. The impact of this method on the optical behavior of the LFR, on the geometrical aspects of the solar field, and on energy production will be investigated using shading and blocking efficiencies, the occupied area by the solar field, the filling factor and through a case study where heat transferred to the outer surface of the absorber tube is evaluated at the city of Riyadh, Kingdom of Saudi Arabia.

2. Methodology

2.1. The alternative method:

This study uses an LFR with ten rows of reflecting mirrors. Each row contains three reflecting mirrors of 3 m in length and 0.5 m in width. The orientation of the solar field is North-South. The receiver is an evacuated tube of 0.125 m in radius and installed 2 m above the primary mirrors with a semi-cylindrical secondary concentrator of 0.25 m in radius.

Each mirror takes a specific tilt to reflect sunlight into the receiver. This tilt varies according to the mirror's position in the solar field and to the sun's position in the sky as described in figure 1.

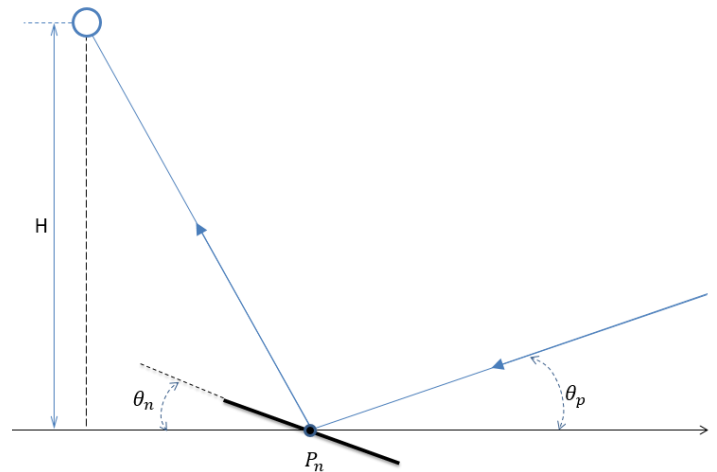


Fig. 1. The reflection process for a given mirror

P_n and θ_n are the position and the tilt of the n^{th} mirror respectively. H is the height of the receiver. θ_p is the sun's profile angle. Equations 1-2 enable the calculation of θ_n and θ_p with γ and α being the azimuth and the elevation angles of the sun respectively:

$$\theta_n = \frac{90 - \theta_p - \tan^{-1}\left(\frac{P_n}{H}\right)}{2} \quad (1)$$

$$\theta_p = 90 - \frac{|\sin(\gamma)|}{\tan(\alpha)} \quad (2)$$

The method presented herein determines the right spacing between reflecting mirrors to avoid mutual shading at a given Design Profile Angle (DPA). To fulfill this purpose, this method is designed according to four simple principals:

- The positions of the two mirrors just beneath the receiver are chosen in order not to have them under the shadow of the secondary concentrator at midday.
- The spacing between the remaining rows is initiated to be equal a fixed minimum spacing.
- Once the DPA is fixed, the spacing between rows is changed two by two to avoid mutual shading between mirrors.
- The minimum spacing between two adjacent mirrors should not be less than 0.05 m to avoid contact between them.

The core of our method relies on the determination of whether mutual shading between adjacent mirrors exists or not using the three cases described in figure 2.

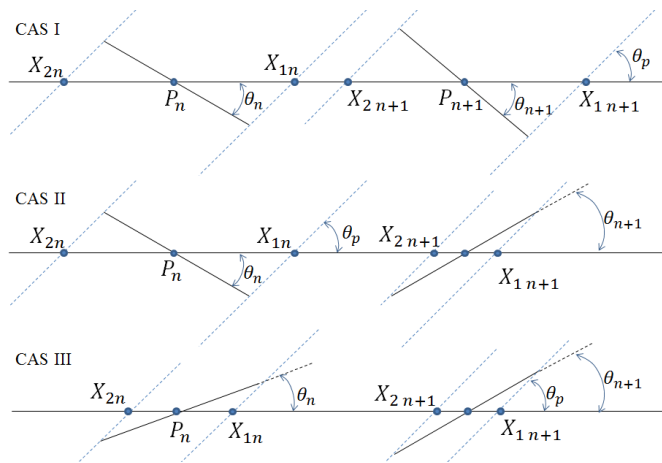


Fig. 2. Possible cases of two adjacent mirrors' tilts

In case I, the tilts of the two mirrors are supposed positive. In this case, equations 3-4 allow the calculation of points X_{1n} and X_{2n} (the same equations apply for $X_{1(n+1)}$ and $X_{2(n+1)}$) with W_m being the mirror's width:

$$X_{1n} = P_n + \frac{W_m \cdot \sin(\theta_p + \theta_n)}{2 \cdot \sin(\theta_p)} \quad (3)$$

$$X_{2n} = P_n - \frac{W_m \cdot \sin(\theta_p + \theta_n)}{2 \cdot \sin(\theta_p)} \quad (4)$$

In case II, the tilt of the first mirror is positive while the tilt of the second one is negative. In this case, X_{1n} and X_{2n} are calculated with equations 3-4 while $X_{1(n+1)}$ and $X_{2(n+1)}$ are calculated using equations 5-6:

$$X_{1(n+1)} = P_{n+1} + \frac{W_m \cdot \sin(\theta_p - |\theta_{n+1}|)}{2 \cdot \sin(\theta_p)} \quad (5)$$

$$X_{2(n+1)} = P_{n+1} - \frac{W_m \cdot \sin(\theta_p - |\theta_{n+1}|)}{2 \cdot \sin(\theta_p)} \quad (6)$$

To avoid shading in cases I and II, it is necessary to have $X_{2(n+1)}$ bigger than X_{1n} .

In case III, the tilts of the two mirrors are negative. In this case, respecting the minimum spacing is sufficient to avoid mutual shading.

The calculation of each mirror's position follows the subsequent logic: the position of the first mirror is determined only by knowing the radius of the secondary concentrator. Then, the spacing between the remaining mirrors is initiated to be equal the minimum spacing (0.05 m). Next, a DPA is fixed to work with. After that, the first two mirrors are chosen and their tilts are calculated using equation 1. Comparing the signs of the two tilts, one of the three cases previously discussed is chosen to calculate X_{1n} and $X_{2(n+1)}$. If $X_{2(n+1)}$ is smaller than X_{1n} , the position of the second mirror is changed and the same previous

calculations are repeated. Otherwise, we move to the next mirror.

Once the positions of all mirrors had been calculated, a correction "h", calculated by equation 7, is added to the nominal height of the secondary concentrator "H" to allow it the acceptance of all reflected sunrays at midday.

$$h = \frac{W_t \left(\frac{\cos \theta_n}{\cos 2\theta_n} \right) - R}{\tan 2\theta_n} \quad (7)$$

W_t is the solar field total width and R is the secondary concentrator's radius.

To assess the impact of our alternative method on the optical performances of the LFR, we chose to analyze two optical effects present in the solar field, namely shading and blocking. These two effects will be evaluated by methods relying on the same mathematical foundations as the alternative method we just discussed. Therefore, the validation of the optimization method will be considered as a proof of the validity of shading and blocking calculations.

In addition, the impact of the present method on the geometrical aspects of the solar field are considered in this work. The variation of the total land occupied by the solar field and of the filling factor are investigated. The filling factor is the ratio of the total reflecting area to the total occupied area. It gives an information of how much the LFR system benefits from the land it is occupying.

2.2. Shading:

The alternative method presented in this work determines the position of each mirror in the solar field in order not to have mutual shading between adjacent mirrors for a fixed DPA. However, the profile angle of the sun changes during the day, which leads to the appearance of shading in the solar field especially when $\theta_p \neq \text{DPA}$. Two sources of shading are identified: the first one is shading caused by a mirror (n+1) on the mirror next to it (n) referred to in this work by (S_n^{n+1}) and calculated using equation 8. The second source is shading of the secondary reflector on a mirror (n) referred to in this work by (S_n^{sc}) and calculated using equations 9-11. Figures 3-4 describe the two possible sources of shading.

$$S_n^{n+1} = \frac{\sin(\theta_p)}{\sin(\theta_p + \theta_n)} (X_{1n} - X_{2n+1}) \quad (8)$$

$$S_n^{sc} = \frac{\sin(\theta_p)}{\sin(\theta_p + \theta_n)} (\min(q_1; X_{1n}) - \max(q_2; X_{2n})) \quad (9)$$

$$q_1 = R - \left(\frac{H}{\tan(\theta_p)} \right) \quad (10)$$

$$q_2 = q_1 - R \left(1 + \frac{1}{\sin(\theta_p)} \right) \quad (11)$$

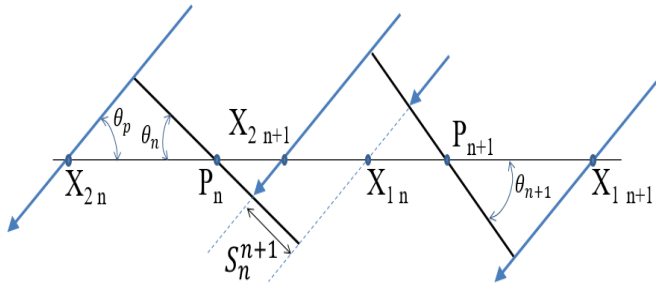


Fig. 3. Mutual shading between two adjacent mirrors

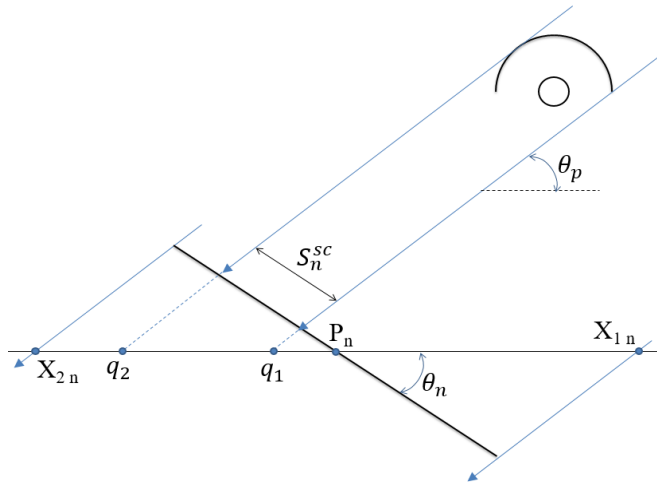


Figure 4: shading of the secondary concentrator on a mirror n

The total amount of shading on a mirror (n), referred to in this work by S_n , can be equal (S_n^{n+1}) or (S_n^{SC}), but also it can be a mixture of the two of them. In this case, it is calculated using equation 12.

$$S_n = S_n^{n+1} + \frac{\sin \theta_p}{\sin(\theta_p + \theta_n)} (q_1 - \max(X_{2n}; q_2)) \quad (12)$$

Equations 13-16 give, respectively, shading efficiency of a mirror, hourly, daily and annual shading efficiencies of the whole LFR.

$$\eta_n^s = 1 - \frac{S_n}{W_m} \quad (13)$$

$$\eta_{hourly}^s = \frac{\sum \eta_n^s}{n} \quad (14)$$

$$\eta_{daily}^s = \frac{1}{t_{ss} - t_{sr}} \int_{t_{sr}}^{t_{ss}} \eta_{hourly}^s dt \quad (15)$$

$$\eta_{yearly}^s = \frac{1}{364} \int_1^{365} \eta_{daily}^s dN \quad (16)$$

Where, t_{sr} and t_{ss} are, respectively, sunrise and sunset times and N is the day number of the year.

2.3. Blocking:

Blocking occurs when a mirror (n) blocks sunrays reflected by the adjacent one (n+1) as described in figure 5. B_n^{n+1} stands for the amount of reflected sunrays being blocked.

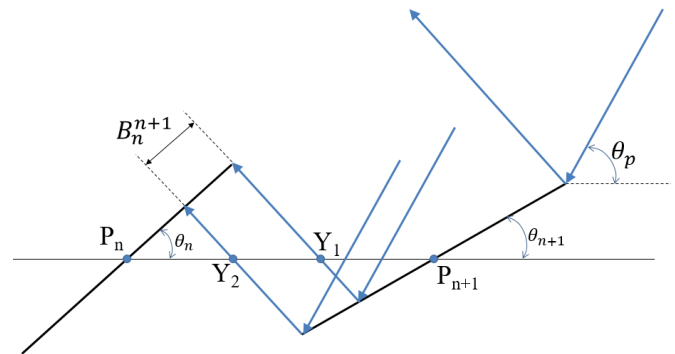


Fig. 5. The blocking process in LFR solar field

Based on figure 5, and using trigonometry, the calculation of blocking follows the subsequent logic: first, $P_n Y_1$ and $P_{n+1} Y_2$ are calculated using equations 17-18. If $P_n Y_2 + P_{n+1} Y_1$ is smaller than $P_n P_{n+1}$ then there is no blocking. Otherwise, blocking exists and it is calculated using equations 19-20.

$$P_n Y_1 = \frac{W_m \sin(180 - \theta_n - \theta_p + 2\theta_{n+1})}{2 \sin(\theta_p - 2\theta_{n+1})} \quad (17)$$

$$P_{n+1} Y_2 = \frac{W_m \sin(180 - \theta_p + \theta_{n+1})}{2 \sin(\theta_p - 2\theta_{n+1})} \quad (18)$$

$$B_n^{n+1} = \frac{W_m}{2} - \left(P_n Y_2 \frac{\sin(\theta_p - 2\theta_{n+1})}{\sin(180 - \theta_n - \theta_p + 2\theta_{n+1})} \right) \quad (19)$$

$$P_n Y_2 = P_n P_{n+1} - P_{n+1} Y_2 \quad (20)$$

Equations 21-24 give, respectively, blocking efficiency of a mirror, hourly, daily and annual blocking efficiencies of the whole LFR.

$$\eta_{n+1}^b = 1 - \frac{B_n^{n+1}}{W_m \sin(\theta_p - \theta_n)} \quad (21)$$

$$\eta_{hourly}^b = \frac{\sum \eta_{n+1}^b}{n} \quad (22)$$

$$\eta_{daily}^b = \frac{1}{t_{ss} - t_{sr}} \int_{t_{sr}}^{t_{ss}} \eta_{hourly}^b dt \quad (23)$$

$$\eta_{yearly}^b = \frac{1}{364} \int_1^{365} \eta_{daily}^b dN \quad (24)$$

2.4. The case study:

At the end of this work, a case study will be discussed to assess the impact of the alternative method presented in this work on energy production of the LFR through the annual mean heat transferred to the outer surface of the absorber tube. To do so, five different cities were compared in terms of annual mean Direct Normal Irradiance resources (DNI). These cities cover a large range of latitudes varying from the

equator to 40° with approximately 10° of difference between two consecutive cities as illustrated in table 1.

Table 1. Information about the considered cities

City	Country	Latitude (φ)	Longitude	Elevation (m)
Accra	Ghana	5.6°	-0.17°	69
Addis Ababa	Ethiopia	8.98°	38.8°	2355
Riyadh	Kingdom of Saudi Arabia	24.7°	46.8°	612
Cairo	Egypt	30.13°	31.4°	74
Madrid	Spain	40.45°	-3.55°	582

DNI data of the five cities were derived from the website www.energyplus.net managed by the National Renewable Energy Laboratory (NREL) [29]. Figure 6 presents the annual mean DNI of the five cities. One may clearly observe that Riyadh has the highest annual mean DNI reaching 500 W/m². Therefore, Riyadh is chosen for the case study.

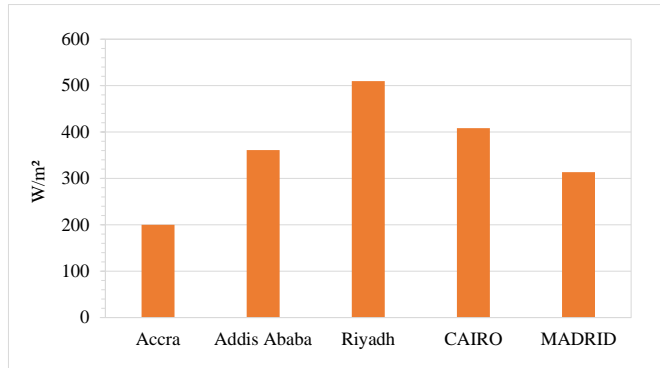


Fig. 6. Annual mean DNI in W/m² for the five considered cities

The annual mean heat transferred to the outer surface of the absorber tube, Q , is evaluated using equation 25 [6], [20], [27]. With IAM_t and IAM_l are the transversal and longitudinal incident angle modifiers respectively. $\eta_o(\theta = 0)$ is the reference optical efficiency calculated at normal incidence angle. A_m is the total solar field area. IAM_t , IAM_l and $\eta_o(\theta = 0)$ are evaluated using the Monte Carlo raytracing software TracePro which is commonly encountered in works that use raytracing technique to evaluate the optical parameters of the LFR [30]–[32].

$$Q = DNI * IAM_t * IAM_l * \eta_o(\theta = 0) * A_m \quad (25)$$

3. Results

3.1. Validation of the alternative method:

To validate our alternative method, a comparison is conducted against the method of J.D. Nixon and P. A. Dives

published in [6] and referred to in this work by N&D. This method is the most suitable for the validation process since it relies on the same principle of optimizing mirrors positions for a fixed DPA to avoid mutual shading. The relative error between mirrors positions obtained by both methods, utilizing equation 26, is used in the comparison process. Results are presented in table 2.

$$\text{relative error} = \frac{|\text{mirror's position by our method} - \text{mirror's position by N\&D}|}{\text{mirror's position by N\&D}} \quad (26)$$

Table 2. Relative error between results obtained using our method and the one of N&D

DPA	P ₁	P ₂	P ₃	P ₄	P ₅
10°	0.000%	0.377%	0.519%	0.545%	0.515%
20°	0.000%	0.744%	0.568%	0.703%	0.773%
30°	0.000%	0.321%	0.368%	0.642%	0.526%
40°	0.000%	0.089%	0.470%	0.355%	0.286%
50°	0.000%	0.848%	0.559%	0.416%	0.332%
60°	0.000%	0.000%	0.000%	0.000%	0.000%
70°	0.000%	0.000%	0.000%	0.000%	0.000%

As is shown by table 2 the overall highest error did not exceed 0.848% in the worst cases proving the validity of our method. In addition, the difference between the two methods declined as the DPA increased. This difference completely disappeared when the DPA exceeded 50°. Indeed, the minimum spacing between adjacent mirrors is reached at very high DPAs, thus mirrors positions are imposed by this restriction rather being calculated by any of the two methods.

Enter alia, no difference between the two methods was reported for mirror number one. In fact, the position of this mirror is not related to the DPA in both methods; it is related to the width of the receiver’s shadow at midday as discussed in section 2.1.

3.2. Impact on geometrical aspects of the solar field:

Figure 7 presents the variation of the filling factor and of the LFR’s total area according to the variation of the DPA. It can be seen that the filling factor increased rapidly from 46.48% to 83.25% when the DPA increased from 10° to 50°. Contrary, and for the same range of variation of the DPA, the LFR’s total area decreased rapidly from 96.82 m² to 54.05 m². After exceeding the DPA of 50°, both the filling factor and the occupied area remained the same: the first one at 83.81% and the second one at 53.69 m².

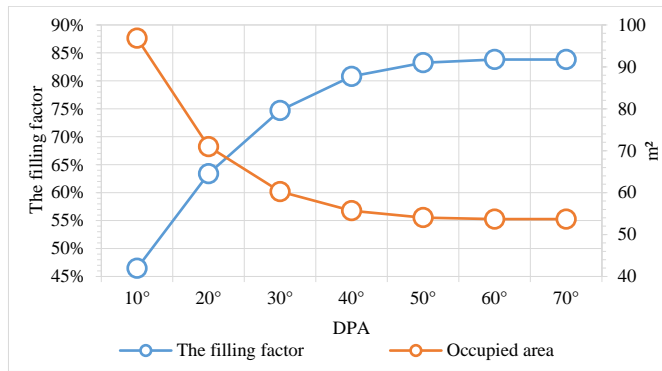


Fig. 7. Variation of the filling factor and of the occupied area with the variation of the DPA

When the DPA increases, the spacing required between mirrors to avoid mutual shading diminishes, leading to a smaller occupied land with high filling factor (since the reflecting area is unchangeable). However, at very high DPAs, the restriction imposed on the minimum spacing between adjacent mirrors is reached. Therefore, no change occurs on the occupied land even the DPA is further increased. Consequently, the filling factor stabilizes. It is important to note that low DPAs lead to larger occupied area but with low filling factor while the opposite is true for high DPAs.

3.3. Impact on shading efficiency:

Figure 8 illustrates the variation of hourly shading efficiency for different DPAs. Reported results are those obtained during the summer solstice. It can be seen that high DPAs had the worst hourly shading efficiency. This results from mirrors being closer to each other when using a high DPA in the optimization process of the solar field. Although, the general trend remained invariable for all DPAs. This trend showed that shading mainly occurred early in the morning and late in the afternoon. While in the middle of the day, shading efficiency was all the time in between 0.8 and 1 but marked with heavy fluctuations. The authors predicted that these fluctuations are the consequence of taking into consideration the secondary concentrator in shading calculations. To make sure of this prediction, shading efficiency was calculated considering only mutual shading between adjacent mirrors in a first time and considering only the influence of shading of the secondary concentrator in a second time. These two shading efficiencies were compared to the overall shading efficiency as described in figure 9.

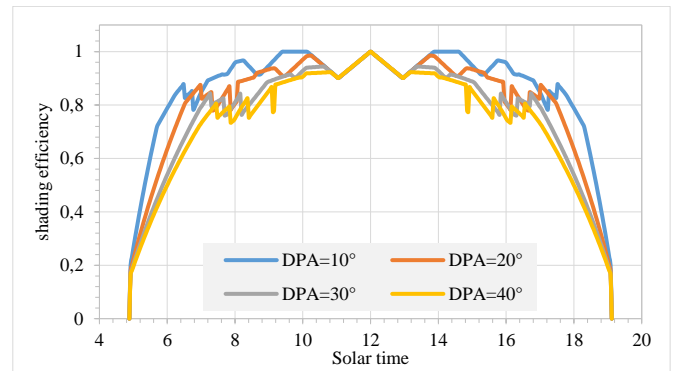


Fig. 8. Variation of hourly shading efficiency for different DPAs

From figure 9 one may divide the first half of a day into three distinguished periods (the same observations are correct for the second part of the day). During the first period that occurred just after sunrise, the overall hourly shading efficiency was exactly equal to shading efficiency due to mutual shading between adjacent mirrors. During this period, there was no shading due to the secondary concentrator. In the second period, both the secondary concentrator and mutual shading between adjacent mirrors contributed to the overall hourly shading efficiency. Throughout the third period, which was the longest one, the overall hourly shading efficiency was influenced only by the secondary concentrator; there was no mutual shading between adjacent mirrors. Fluctuations registered in this period are due to the nature of the interaction between shading of the secondary concentrator and reflecting mirrors of the solar field. In fact, when the secondary concentrator casts its shadow on the solar field, three cases are possible:

- The first case is when a whole mirror or part of it is under the shadow of the secondary concentrator.
- The second case is when the whole shadow of the secondary concentrator falls on the spacing between two adjacent mirrors. In this case, it is like if shading does not occur and shading efficiency will equal 1. The impact of this case is clearly observed during some short periods during the middle of the day as reported in figure 9.
- The third case is when shading of the secondary concentrator falls on parts of two adjacent mirrors as well as the spacing between them.

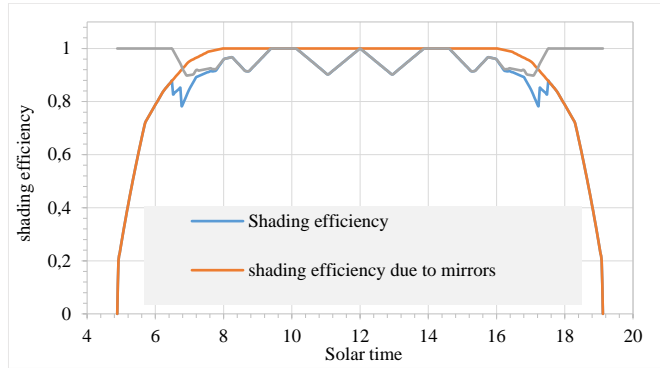


Fig. 9. Variation of hourly shading efficiency and of shading efficiencies due only to mutual shading between mirrors and due only to the secondary concentrator

Figure 10 depicts the variation of daily shading efficiency for different latitudes. Reported results are those obtained with $DPA=10^\circ$. It can be observed that the general trend of daily shading efficiency represented two extrema, a maximum during the summer and a minimum during the winter. Nevertheless, the difference between these extrema did not exceed 6% in the worst cases. This difference lessened when the latitude decreased until it disappeared at the equator that had the best results.

The seasonal variation of shading is a direct result of the considerable variation in the sun elevation in the sky along the year leading to higher incidence angle during the summer days, thus higher shading efficiency. Yet, the elevation of the sun in the sky does not vary much at low latitude locations.

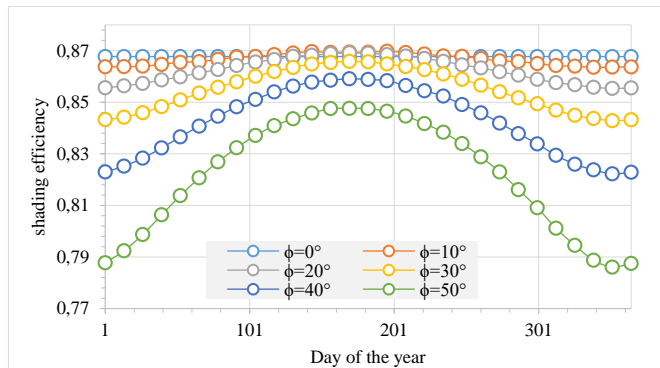


Fig. 10. Variation of daily shading efficiency during a year for different latitudes ($DPA=10^\circ$)

It is worth noting that Vashi Sharma reported the same conclusions about the seasonal variation of shading in his work published in [33] but relying on a monthly basis. In addition, results reported herein concerning variation of shading according to latitude confirms what was concluded in a recent paper published by the same aforementioned author [23].

Figure 11 gives information about the variation of annual shading efficiency for different DPAs at latitudes varying between 0° and 50° . As the figure shows, better results are recorded at low latitudes using low DPAs. Annual efficiency as high as 85.75% is reported at the equator for $DPA=10^\circ$. Besides, it is observed that annual shading efficiency diminished as the latitude increased. Yet, this decrease was not significant until the latitude of 20° was exceeded. The overall decline in annual efficiency over the studied range of latitudes was equal 6.73% in the case of $DPA=40^\circ$, which was the worst one, while it was as low as 4.54% in the case of $DPA=10^\circ$.

The annual shading efficiency comes to confirm what was reported in the analysis of hourly and daily shading efficiencies; the best efficiencies will be achieved at low latitude locations using low DPAs. However, it revealed two more important information. The first one is that shading efficiency remains constant at low latitude locations (smaller than 20°) where the highest efficiencies are reported. Whereas the second observation is that low DPAs not only enable the LFR get to better results, but also it makes its performance in terms of shading efficiency less dependent on the location where it is installed.

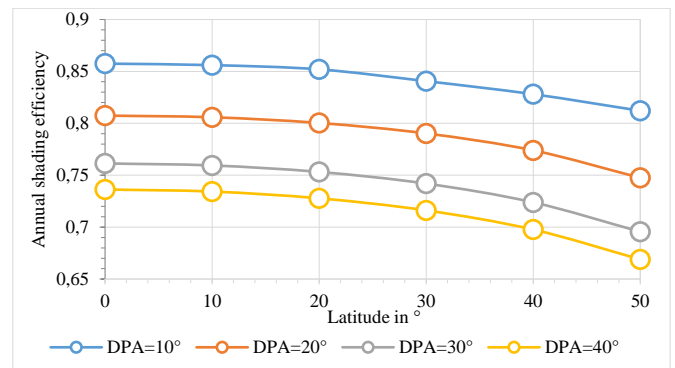


Fig. 11. Variation of annual shading efficiency for different DPA according to latitude

3.4. Impact on blocking efficiency:

Figure 12 shows the hourly variation of blocking efficiency for different DPAs. It is clear from the figure that blocking only occurred for a short period around midday. This period became larger when high DPAs were used. The deepest decrease in blocking efficiency was always observed at noon and it was less important in the case of low DPAs.

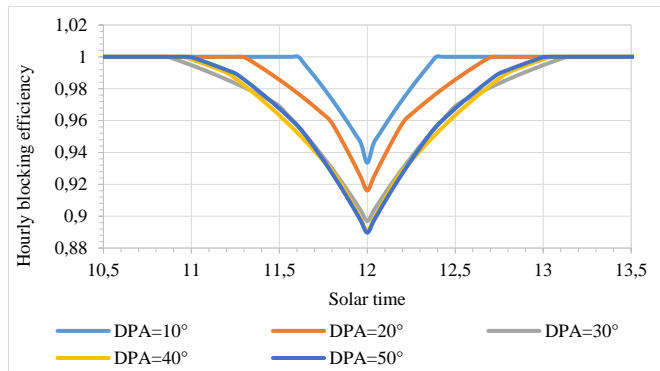


Fig. 12. Variation of hourly blocking efficiency for different DPA

These results came in accordance with what was concluded by Vashi Sharma who reported that blocking losses are maximum at noon and zero near sunrise and sunset [33]. This behavior is a result of the variation in the incidence angle of the sun throughout the day. This variation not only influences the path of incoming and reflected sunrays but also it modifies the tilt of each mirror in the solar field. In fact, higher incidence angles are reached around midday, which implies bigger tilts maximizing the odds that blocking occurs. This is further aggravated with tight solar fields as in the case of high DPAs.

The variation of daily blocking efficiency is plotted against the variation of the location's latitude in figure 13. Reported results are those obtained for DPA=30°. The figure shows that blocking had a season related behavior at high latitudes recording a maximum in the winter and a minimum in the summer but it was more stable at low latitudes. However, the change in daily blocking efficiency is insignificant since the registered efficiencies were all the year above 99% at every location. The main reason behind this compartment is that in a daily basis, unlike the hourly basis, tilts of the reflecting mirrors do not change much.

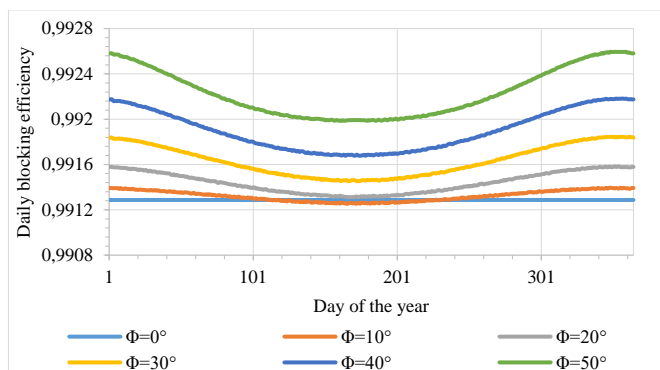


Fig. 13. Variation of daily blocking efficiency during a year for different latitudes (DPA=30°)

Figure 14 illustrates the change in annual blocking efficiency according to different DPAs and different latitudes. As in the case of shading efficiency, the annual efficiency confirms the results obtained during the hourly and daily analysis. It can be seen from the figure that better results are achieved at high latitudes especially when using a low DPA. In addition, it is reported, once more, that blocking efficiency was above 99% in all cases.

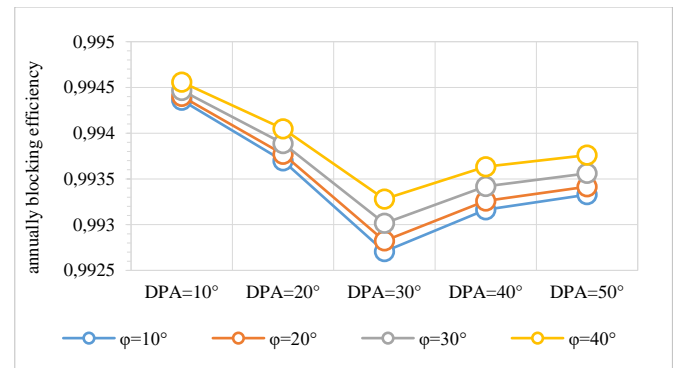


Fig. 14. Variation of annual blocking efficiency for different DPAs and for different latitudes

When comparing the results concerning shading and blocking efficiencies one may first deduce that blocking is much less important than shading. On the other hand, the two efficiencies have an opposite behavior on hourly and daily basis. In fact, hourly shading efficiency is maximum in the middle of the day when the sun is high in the sky unlike blocking efficiency that is maximum around sunrise and sunset. In addition, the behavior of both efficiencies is related to the variation in seasons with shading efficiency being maximum in the summer when blocking efficiency is minimum while the opposite is true in the winter.

Changing the used DPA also affects shading and blocking efficiencies. Both efficiencies are maximized with low DPAs. However, annual blocking efficiency remains above 99% despite the used DPA.

3.5. Case study:

Figure 15 describes the change in $\eta_o(\theta = 0)$ according to DPA alongside with the variation in the annual available power which equals $DNI \cdot A_m$. It is observed that $\eta_o(\theta = 0)$ rose from 11.088% at DPA=10° to 23.562% at DPA=50° while the annual available power went down from 49346 W to 27548 W over the same range of variation in DPA. At low DPAs, the LFR had higher available power but with low $\eta_o(\theta = 0)$. By contrast, at high DPAs it had better $\eta_o(\theta = 0)$ however with low available power.

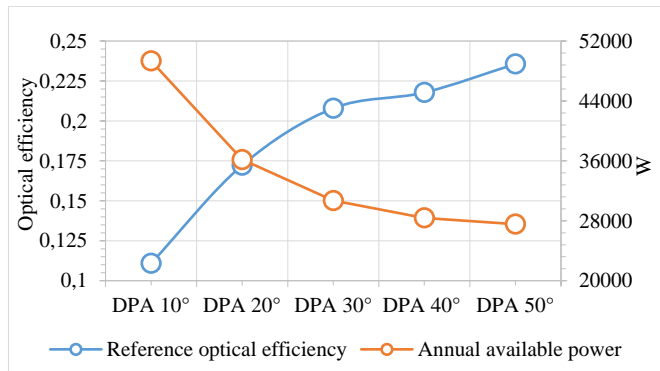


Fig. 15. Variation of the annual available power and of $\eta_o(\theta = 0)$ with the variation of DPA

The trend of the available power is nothing more than the image of that of the occupied area. This was highly expected since, by definition, the available power is the multiplication of the occupied area by a constant, which is the annual available DNI. On the other hand, working with a low DPA leads to bigger spacing between adjacent mirrors. This results in more sunrays being lost in this spacing penalizing $\eta_o(\theta = 0)$. The opposite thing can be said for high DPAs.

Figure 16 presents the variation of the annual heat transferred according to the DPA. As can be seen modifying the used DPA did not have significantly effect on the annual performance of the LFR; comparable annual heat transferred was recorded by all DPAs. The authors did not expect this behavior at the beginning of this work. Although, the analysis of obtained results all along this study, especially the discussion of figure 15, made it sound normal. Indeed, using low DPAs requires bigger spacing to avoid mutual shading between adjacent mirrors. This results in a larger occupied area that will certainly benefits from high available power but it cannot make complete use of it for two main reasons: a low filling factor and a low optical efficiency. Contrary, with high DPAs, higher filling factor and optical efficiency are achieved but they are penalized by low available power. This contradiction makes both cases end with approximately the same transferred heat to the outer surface of the absorber tube. Owing to this fact, it is concluded that high DPAs are the most suitable to be used since they lead to the same annual performance as the other DPAs with smaller occupied land, thus lower capital cost. However, with high DPAs, the spacing between reflecting mirrors tend to become uniform across the solar field and at the end it becomes nothing more than the minimum spacing imposed by the method. This fact makes the whole process of developing new complex methods to optimize mirrors' positions questionable. Instead, the authors think the use of equidistant spacing between adjacent mirrors is sufficient to get to satisfying results.

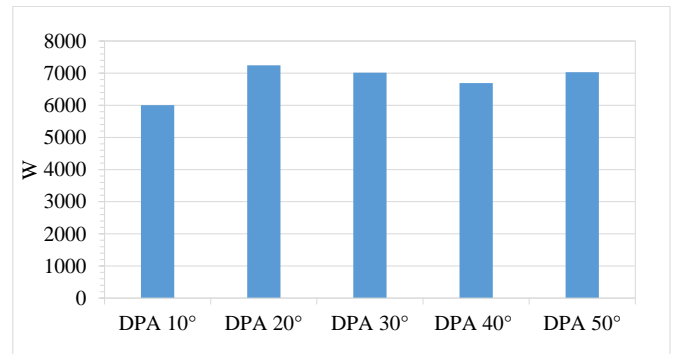


Fig. 16. Variation of the annual heat transferred to the outer surface of the absorber tube according to the variation of DPA

4. Conclusion

In the present work, an alternative method to optimize the LFR's solar field was discussed and successfully validated. The impact of this method on the LFR's optical behavior, on the geometrical aspects of the solar field and on energy production was considered and the following conclusions can be derived:

- Blocking is not as important as shading.
- Blocking and shading have an opposite hourly and daily behavior; when one is maximum, the other is minimum.
- Using a low DPA in the optimization process leads to better shading and blocking efficiencies but also leads to larger occupied area with a poor filling factor.
- Comparable annual mean heat transferred to the outer surface of the absorber tube was achieved by all DPAs which lead the authors to conclude that the use of equidistant spacing between adjacent mirrors is sufficient to get to satisfying results without the need to develop any new or complex optimizing methods.

In this work, the authors studied the impact of the alternative method on each parameter separately. In upcoming works, the others will address this problem using a multi-objective optimization algorithm considering all the parameters presented in this work as well as exergy and the nature of the Heat Transfer Fluid circulating in the absorber tube. In addition, the impact of the working fluid and of the power block itself on the LFR's overall performances will be evaluated.

Acknowledgement

The authors would like to thank the "Centre National pour la Recherche Scientifique et Technique CNRST" for the grant it is offering to Elmaanaoui Youssef under the number 007UH2C2014.

References:

- [1] R. Abbas, M. J. Montes, A. Rovira, and J. M. Martínez-Val, "Parabolic trough collector or linear Fresnel collector? A comparison of optical features including thermal quality based on commercial solutions," *Sol. Energy*, vol. 124, pp. 198–215, Feb. 2016.
- [2] R. Abbas and J. M. Martínez-Val, "Analytic optical design of linear Fresnel collectors with variable widths and shifts of mirrors," *Renew. Energy*, vol. 75, pp. 81–92, Mar. 2015.
- [3] S. Benyakhlef, A. Al Mers, O. Merroun, A. Bouatem, N. Boutammachte, S. El Alj, H. Ajdad, Z. Erregueragui, and E. Zemmouri, "Impact of heliostat curvature on optical performance of Linear Fresnel solar concentrators," *Renew. Energy*, vol. 89, pp. 463–474, Apr. 2016.
- [4] M. J. Montes, C. Rubbia, R. Abbas, and J. M. Martínez-Val, "A comparative analysis of configurations of linear Fresnel collectors for concentrating solar power," *Energy*, vol. 73, pp. 192–203, Aug. 2014.
- [5] J. D. Nixon, P. K. Dey, and P. A. Davies, "Design of a novel solar thermal collector using a multi-criteria decision-making methodology," *J. Clean. Prod.*, vol. 59, pp. 150–159, Nov. 2013.
- [6] J. D. Nixon and P. A. Davies, "Cost-exergy optimisation of linear Fresnel reflectors," *Sol. Energy*, vol. 86, no. 1, pp. 147–156, Jan. 2012.
- [7] R. Abbas, J. M. Martínez-Val, J. Muñoz-Antón, M. Valdés, A. Ramos, A. Rovira, M. J. Montes, H. Sait, R. Muñoz, Á. Gamarra, and M. Villén, "A Quest to the Cheapest Method for Electricity Generation in Concentrating Solar Power Plants," *Energy Procedia*, vol. 75, pp. 514–520, Aug. 2015.
- [8] R. Abbas, J. Muñoz-Antón, M. Valdés, and J. M. Martínez-Val, "High concentration linear Fresnel reflectors," *Energy Convers. Manag.*, vol. 72, pp. 60–68, Aug. 2013.
- [9] R. Abbas and J. M. Martínez-Val, "A comprehensive optical characterization of linear Fresnel collectors by means of an analytic study," *Appl. Energy*, Feb. 2016.
- [10] D. Barlev, R. Vidu, and P. Stroeve, "Innovation in concentrated solar power," *Sol. Energy Mater. Sol. Cells*, vol. 95, no. 10, pp. 2703–2725, Oct. 2011.
- [11] D. Cocco and G. Cau, "Energy and economic analysis of concentrating solar power plants based on parabolic trough and linear Fresnel collectors," *Proc. Inst. Mech. Eng. Part J. Power Energy*, vol. 229, no. 6, pp. 677–688, Sep. 2015.
- [12] A. Giotri, M. Binotti, P. Silva, E. Macchi, and G. Manzoloni, "Comparison of Two Linear Collectors in Solar Thermal Plants: Parabolic Trough vs Fresnel," 2011, pp. 621–630.
- [13] G. Morin, J. Dersch, W. Platzer, M. Eck, and A. Häberle, "Comparison of Linear Fresnel and Parabolic Trough Collector power plants," *Sol. Energy*, vol. 86, no. 1, pp. 1–12, Jan. 2012.
- [14] R. Abbas, M. J. Montes, M. Piera, and J. M. Martínez-Val, "Solar radiation concentration features in Linear Fresnel Reflector arrays," *Energy Convers. Manag.*, vol. 54, no. 1, pp. 133–144, Feb. 2012.
- [15] J. Muñoz-Antón, R. Abbas, J. Martínez-Val, and M. Montes, "Going further with Fresnel Receiver: New Design Window for Direct Steam Generation," *Energy Procedia*, vol. 49, pp. 184–192, 2014.
- [16] R. Muñoz, J. M. Martínez-Val, R. Abbas, J. Muñoz-Antón, A. Rovira, and M. J. Montes, "A Concentrating Solar Power Prototype for validating a new Fresnel-based plant design," *Energy Procedia*, vol. 75, pp. 423–429, Aug. 2015.
- [17] J. Zhu and H. Huang, "Design and thermal performances of Semi-Parabolic Linear Fresnel Reflector solar concentration collector," *Energy Convers. Manag.*, vol. 77, pp. 733–737, Jan. 2014.
- [18] S. Balaji, K. S. Reddy, and T. Sundararajan, "Optical modelling and performance analysis of a solar LFR receiver system with parabolic and involute secondary reflectors," *Appl. Energy*, vol. 179, pp. 1138–1151, Oct. 2016.
- [19] S. S. Sahoo, S. Singh, and R. Banerjee, "Thermal hydraulic simulation of absorber tubes in linear Fresnel reflector solar thermal system using RELAP," *Renew. Energy*, vol. 86, pp. 507–516, Feb. 2016.
- [20] N. B. Desai and S. Bandyopadhyay, "Integration of parabolic trough and linear Fresnel collectors for optimum design of concentrating solar thermal power plant," *Clean Technol. Environ. Policy*, vol. 17, no. 7, pp. 1945–1961, Oct. 2015.
- [21] O. A. Hamed, H. Kosaka, K. H. Bamardouf, K. Al-Shail, and A. S. Al-Ghamdi, "Concentrating solar power for seawater thermal desalination," *Desalination*, vol. 396, pp. 70–78, Oct. 2016.
- [22] H. H. Sait, J. M. Martinez-Val, R. Abbas, and J. Munoz-Anton, "Fresnel-based modular solar fields for performance/cost optimization in solar thermal power plants: A comparison with parabolic trough collectors," *Appl. Energy*, vol. 141, pp. 175–189, Mar. 2015.
- [23] V. Sharma, J. K. Nayak, and S. B. Kedare, "Effects of shading and blocking in linear Fresnel reflector field," *Sol. Energy*, vol. 113, pp. 114–138, Mar. 2015.
- [24] D. R. Mills and G. L. Morrison, "Compact linear Fresnel reflector solar thermal powerplants," *Sol. Energy*, vol. 68, no. 3, pp. 263–283, 2000.
- [25] D. R. Mills and G. L. Morrison, "Modelling study for compact Fresnel reflector power plant," *J. Phys. IV*, vol. 9, no. PR3, p. Pr3-159-Pr3-165, Mar. 1999.
- [26] A. Barbón, N. Barbón, L. Bayón, and J. A. Otero, "Optimization of the length and position of the

- absorber tube in small-scale Linear Fresnel Concentrators,” *Renew. Energy*, vol. 99, pp. 986–995, Dec. 2016.
- [27] J. D. Nixon, P. K. Dey, and P. A. Davies, “Design of a novel solar thermal collector using a multi-criteria decision-making methodology,” *J. Clean. Prod.*, vol. 59, pp. 150–159, Nov. 2013.
- [28] J. Chaves and M. Collares-Pereira, “Etendue-matched two-stage concentrators with multiple receivers,” *Sol. Energy*, vol. 84, no. 2, pp. 196–207, Feb. 2010.
- [29] “EnergyPlus | EnergyPlus.” [Online]. Available: <https://www.energyplus.net/>. [Accessed: 02-Jun-2016].
- [30] F. Chen, M. Li, R. Hassanien Emam Hassanien, X. Luo, Y. Hong, Z. Feng, M. Ji, and P. Zhang, “Study on the Optical Properties of Triangular Cavity Absorber for Parabolic Trough Solar Concentrator,” *Int. J. Photoenergy*, vol. 2015, pp. 1–9, 2015.
- [31] M. Lin, K. Sumathy, Y. J. Dai, R. Z. Wang, and Y. Chen, “Experimental and theoretical analysis on a linear Fresnel reflector solar collector prototype with V-shaped cavity receiver,” *Appl. Therm. Eng.*, vol. 51, no. 1–2, pp. 963–972, Mar. 2013.
- [32] W. T. Xie, Y. J. Dai, and R. Z. Wang, “Numerical and experimental analysis of a point focus solar collector using high concentration imaging PMMA Fresnel lens,” *Energy Convers. Manag.*, vol. 52, no. 6, pp. 2417–2426, Jun. 2011.
- [33] V. Sharma, “Hourly and Monthly Variation in Shading and Blocking of Aperture Area in a Linear Fresnel Reflector Field,” *Energy Procedia*, vol. 48, pp. 233–241, 2014.
- [34] M. H. Ahmed, M. Rady, A. M. A. Amin, F. M. Montagnino and F. Paredes, "Comparison of thermal and optical performance of Linear Fresnel and Parabolic Trough Concentrator," 2015 International Conference on Renewable Energy Research and Applications (ICRERA), Palermo, 2015, pp. 626-629.